

Quantum spin stabilized magnetic levitation in the presence of dissipation

Katja Kustura,^{1,2,*} Vanessa Wachter,^{3,4} Adrián E. Rubio López,^{1,2} and Cosimo C. Rusconi^{5,6,†}

¹*Institute for Quantum Optics and Quantum Information of the Austrian Academy of Sciences, A-6020 Innsbruck, Austria.*

²*Institute for Theoretical Physics, University of Innsbruck, A-6020 Innsbruck, Austria.*

³*Max Planck Institute for the Science of Light, Staudtstraße 2, 91058 Erlangen, Germany*

⁴*Department of Physics, University of Erlangen-Nürnberg, Staudtstraße 7, 91058 Erlangen, Germany*

⁵*Max-Planck-Institut für Quantenoptik, Hans-Kopfermann-Strasse 1, 85748 Garching, Germany.*

⁶*Munich Center for Quantum Science and Technology,
Schellingstrasse 4, D-80799 München, Germany.*

(Dated: June 29, 2021)

In the absence of dissipation a non-rotating magnetic nanoparticle can be stably levitated in a static magnetic field as a consequence of the spin origin of its magnetization. Here, we study the effects of dissipation on the stability of the system, considering the interaction with the background gas and the intrinsic Gilbert damping of magnetization dynamics. We find that dissipation limits the time over which a particle can be stably levitated. At large applied magnetic fields we identify magnetization switching induced by Gilbert damping as the key limiting factor for stable levitation. At low applied magnetic fields and for small particle dimensions magnetization switching is prevented due to the strong coupling of rotation and magnetization dynamics, and the stability is mainly limited by the gas-induced dissipation. In this latter case, high vacuum should be sufficient to extend stable levitation over experimentally relevant timescales. Our results demonstrate the possibility to experimentally observe the phenomenon of quantum spin stabilized magnetic levitation.

The Einstein–de Haas [1, 2] and Barnett effects [3] are macroscopic manifestations of the internal angular momentum origin of magnetization: a change in the magnetization causes a change in the mechanical rotation and conversely. Because of the reduced moment of inertia of levitated nano- to microscale particles, these effects play a dominant role in the dynamics of such systems [4–10]. This offers the possibility to harness these effects for a variety of applications such as precise magnetometry [11–16], inertial sensing [17, 18], coherent spin-mechanical control [19, 20], and spin-mechanical cooling [21, 22] among others. Notable in this context is the possibility to stably levitate a ferromagnetic particle in a static magnetic field [23, 24]. Stable levitation is enabled by the internal angular momentum origin of the magnetization which, even in the absence of mechanical rotation, provides the required angular momentum to gyroscopically stabilize the system. Such a phenomenon, which we refer to as quantum spin stabilized levitation to distinguish it from the rotational stabilization of magnetic tops [25–27], relies on the conservative interchange between internal and mechanical angular momentum. Omnipresent dissipation, however, exerts additional non-conservative torques on the system which might alter the delicate gyroscopic stability [26, 28]. It thus remains to be determined if stable levitation can be observed under realistic conditions, where dissipative effects cannot be neglected.

In this letter, we address this question. Specifically, we consider the dynamics of a levitated magnetic nanoparticle (nanomagnet hereafter) in a static magnetic field in the presence of dissipation originating

both from the collisions with the background gas and from the intrinsic damping of magnetization dynamics (Gilbert damping) [29, 30], which are expected to be the dominant sources of dissipation for levitated nanomagnets [8, 13, 31–33]. We find that the system can be levitated for a finite time before losing stability, as generally expected for gyroscopically stabilized systems [28]. Confined dynamics can be observed only when the time over which the nanomagnet is levitated is longer than the period of center-of-mass oscillations in the magnetic trap. When this is the case, we define the system to be metastable. The levitation time and the mechanism behind the instability depend on the parameter regime of the system. We identify two relevant regimes, which correspond to the two cases in which a non-rotating nanomagnet can be stably levitated in the absence of dissipation [23, 24]. First, at large applied magnetic fields the intrinsic Gilbert damping induces magnetization switching, which leads to instability on a timescale shorter than the period of center-of-mass oscillations. Second, at weak applied magnetic fields and for small particle dimensions, the system loses stability through the interaction with the background gas on a much longer timescale than the period of center-of-mass oscillations. In this latter case, the levitation time can be extended in high vacuum, thus allowing, in principle, the unambiguous experimental observation of quantum spin stabilized magnetic levitation.

We consider a single domain nanomagnet levitated in a static magnetic field $\mathbf{B}(\mathbf{r})$ as shown schematically in Fig. 1(a). The nanomagnet is modelled as a spheroidal rigid body of mass density ρ_M and semi-axes lengths a, b ($a > b$), having uniaxial magnetocrystalline anisotropy, with the anisotropy axis assumed to be along the major semi-axis a [34]. We assume that the magnetic response of the nanomagnet is approximated by a point

* katja.kustura@uibk.ac.at

† cosimo.rusconi@mpq.mpg.de

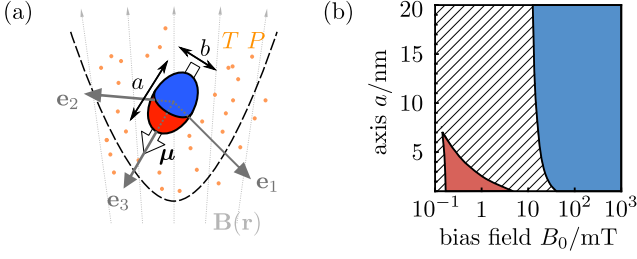


Figure 1. (a) Illustration of a spheroidal nanomagnet levitated in an external field $\mathbf{B}(\mathbf{r})$ and surrounded by a gas at the temperature T and the pressure P (orange). (b) Linear stability diagram of a non-rotating nanomagnet in the absence of dissipation. Blue (red) region denotes the stable atom (Einstein–de Haas) phase; hatched area is the unstable region. The following values are used: $a/b = 2$, $\rho_M = 10^4 \text{ kg/m}^3$, $k_a = 10^4 \text{ J/m}^3$, $\gamma_0 = 1.76 \times 10^{11} \text{ rad/(sT)}$, $B' = 10^4 \text{ T/m}$, and $B'' = 10^6 \text{ T/m}^2$. We calculate the magnitude of the magnetic moment as $\mu = \rho_\mu V$, where $\rho_\mu = [\rho_M \mu_B / (50 \text{ amu})] \text{ J/(Tm}^3)$, with μ_B the Bohr magneton and amu the atomic mass unit.

dipole with magnetic moment $\boldsymbol{\mu}$ of constant magnitude $\mu \equiv |\boldsymbol{\mu}|$, as it is often justified for single domain particles [34, 35]. The magnetic moment $\boldsymbol{\mu}$ is related to the internal angular momentum \mathbf{F} by the gyromagnetic relation $\boldsymbol{\mu} = \gamma_0 \mathbf{F}$, where γ_0 is the gyromagnetic ratio of the material [36]. The orientation of the nanomagnet is described by the body-fixed reference frame $O\mathbf{e}_1\mathbf{e}_2\mathbf{e}_3$, which is obtained from the laboratory frame $O\mathbf{e}_x\mathbf{e}_y\mathbf{e}_z$ according to $(\mathbf{e}_1, \mathbf{e}_2, \mathbf{e}_3)^T = R(\boldsymbol{\Omega})(\mathbf{e}_x, \mathbf{e}_y, \mathbf{e}_z)^T$, where $\boldsymbol{\Omega} = (\alpha, \beta, \gamma)^T$ are the Euler angles and $R(\boldsymbol{\Omega})$ is the rotational matrix (see Appendix A). The body-fixed reference frame is chosen such that \mathbf{e}_3 coincides with the anisotropy axis. The relevant degrees of freedom of the system are the center-of-mass position \mathbf{r} and momentum \mathbf{p} , the mechanical angular momentum \mathbf{L} , the orientation of the nanomagnet $O\mathbf{e}_1\mathbf{e}_2\mathbf{e}_3$, and the magnetic moment $\boldsymbol{\mu}$. We hereafter consider a Ioffe-Pritchard magnetic trap [37], given by $\mathbf{B}(\mathbf{r}) = \mathbf{e}_x[B_0 + B''x^2/2 - B''(y^2 + z^2)/4] - \mathbf{e}_y(B'y + B''xy/2) + \mathbf{e}_z(B'z - B''xz/2)$, where B_0, B' and B'' are, respectively, the field bias, gradient and curvature [38]. In the following it is convenient to define dimensionless variables: the center-of-mass variables $\tilde{\mathbf{r}} \equiv \mathbf{r}/a$, $\tilde{\mathbf{p}} \equiv \gamma_0 a \mathbf{p}/\mu$, the mechanical angular momentum $\boldsymbol{\ell} \equiv \gamma_0 \mathbf{L}/\mu$, the magnetic moment $\mathbf{m} \equiv \boldsymbol{\mu}/\mu$, and the magnetic field $\mathbf{b}(\tilde{\mathbf{r}}) \equiv \mathbf{B}(a\tilde{\mathbf{r}})/B_0$.

The dynamics of the nanomagnet in the laboratory frame are given by the equations of motion

$$\dot{\tilde{\mathbf{r}}} = \omega_I \tilde{\mathbf{p}}, \quad (1)$$

$$\dot{\tilde{\mathbf{p}}} = \omega_L \nabla_{\tilde{\mathbf{r}}} [\mathbf{m} \cdot \mathbf{b}(\tilde{\mathbf{r}})] - \Gamma_{\text{cm}} \tilde{\mathbf{p}}, \quad (2)$$

$$\dot{\boldsymbol{\ell}} = \omega_L \mathbf{m} \times \mathbf{b}(\tilde{\mathbf{r}}) - \dot{\mathbf{m}} - \Gamma_{\text{rot}} \boldsymbol{\ell}, \quad (3)$$

$$\dot{\mathbf{e}}_3 = \boldsymbol{\omega} \times \mathbf{e}_3, \quad (4)$$

$$\dot{\mathbf{m}} = \frac{\mathbf{m}}{1 + \eta_G^2} \times [\boldsymbol{\omega}_{\text{eff}} - \eta_G \mathbf{m} \times (\boldsymbol{\omega} + \boldsymbol{\omega}_{\text{eff}} + \eta_G \boldsymbol{\omega} \times \mathbf{m})]. \quad (5)$$

Here $\omega_I \equiv \mu/(\gamma_0 M a^2)$ is the Einstein–de Haas frequency,

with M the mass of the nanomagnet, $\omega_L \equiv \gamma_0 B_0$ is the Larmor frequency, $\boldsymbol{\omega} \equiv I^{-1} \mathbf{L}$ is the angular velocity, with I the tensor of inertia, and $\boldsymbol{\omega}_{\text{eff}} \equiv 2\omega_A (\mathbf{m} \cdot \mathbf{e}_3) \mathbf{e}_3 + \omega_L \mathbf{b}(\tilde{\mathbf{r}})$, with the anisotropy frequency $\omega_A \equiv k_a V \gamma_0 / \mu$, where V is the volume of the nanomagnet and k_a denotes the material dependent anisotropy constant [35]. Eqs. (1-4) describe the center-of-mass and rotational dynamics of a rigid body in the presence of dissipation induced by the background gas, described by the center-of-mass (rotational) friction tensor Γ_{cm} (Γ_{rot}) [32]. The expressions for $\Gamma_{\text{cm,rot}}$ depend on the particle shape. Here we take the expressions derived in [32] for a cylindrical particle [39]. The tensors $\Gamma_{\text{cm,rot}}$ depend on the gas properties, namely the pressure P , the temperature T and the molar mass \mathcal{M} , and on the ratio of the surface and the bulk temperature of the particle, which we assume to be equal to the gas temperature, namely $T_{\text{surface}} = T_{\text{bulk}} = T$. Furthermore, they account for two different scattering processes, namely the specular and the diffusive reflection of the gas from the particle, which is described by a phenomenological interpolation coefficient α_c [32]. The magnetization dynamics Eq. (5) is the Landau-Lifshitz-Gilbert equation in the laboratory frame [8, 40], with the effective magnetic field $\boldsymbol{\omega}_{\text{eff}}/\gamma_0$ and the Gilbert damping parameter η_G [29, 41]. Eqs. (1-5) describe the classical dynamics of a levitated nanomagnet where the effect of the spin origin of magnetization, namely the gyromagnetic relation, is taken into account phenomenologically by Eq. (5) [24] (see Appendix B). Here we neglect the effects of stochastic noise which, for sufficiently low temperatures, are expected not to alter the deterministic effects captured by Eqs. (1-5) (see below). An equilibrium solution of Eqs. (1-5) is given by $\tilde{\mathbf{r}} = \tilde{\mathbf{p}} = \boldsymbol{\ell} = 0$ and $\mathbf{e}_3 = \mathbf{m} = -\mathbf{e}_x$. This corresponds to the configuration in which the nanomagnet is fixed at the trap center, with the magnetic moment along the anisotropy axis and anti-aligned to the bias field B_0 . This equilibrium point is linearly stable in the absence of dissipation [23, 24], with an example of a stability diagram shown in Fig. 1(b).

The initial conditions for the dynamics in Eqs. (1-5), namely at the time $t = 0$, depend on the initial state of the particle, which is determined by the loading scheme and the preparation of a nanomagnet in the magnetic trap. We assume that the nanomagnet is prepared in the thermal state of a Hamiltonian \mathcal{H}_{aux} at the temperature T , where we consider an auxiliary loading potential described by $\mathcal{H}_{\text{aux}} = \mathcal{H}_{\text{cm}} + \mathcal{H}_{\text{rot}} + \mathcal{H}_\mu$. We assume harmonic trapping of the center of mass according to $\mathcal{H}_{\text{cm}} \equiv \mathbf{p}^2/(2M) + M[\omega_X^2 r_x^2 + \omega_Y^2 (r_y^2 + r_z^2)]/2$, where we take $\omega_X^2 = \mu B''/M$ and $\omega_Y^2 = \mu(B'^2 - B_0 B''/2)/(M B_0)$ in agreement with the typical trapping frequencies in a Ioffe-Pritchard field [38]. The rotational dynamics is given by $\mathcal{H}_{\text{rot}} \equiv \mathbf{L} I^{-1} \mathbf{L}/2 - k_a V e_{3,x}^2$, where the confining potential is supplied by the anisotropy. The magnetic moment is polarized along an external applied field according to $\mathcal{H}_\mu \equiv -\mu_x B_0$. For each degree of freedom we take the corresponding standard deviation as the initial displacement from the equilibrium (see Appendix C). The initial

conditions are parametrized by the temperature T , with the loading potential \mathcal{H}_{aux} that models general trapping schemes used to trap magnetic particles (see below).

Linear stability analysis of Eqs. (1-5) shows that the system is unstable. When the nanomagnet is metastable, however, it is still possible for it to levitate for an extended time before being eventually lost from the trap, as is the case for the classical magnetic top [25–27]. In the following we investigate this possibility by solving numerically Eqs. (1-5) in the two stable regions derived in the absence of dissipation [Fig. 1(b)]: (i) the *atom phase* at large magnetic fields, and (ii) the *Einstein–de Haas phase* at small particle dimensions and weak magnetic fields.

Atom phase denotes the regime where $\omega_L \gg \omega_A, \omega_I$, which can be achieved for sufficiently large values of the bias field B_0 . In this regime the coupling of the magnetic moment $\boldsymbol{\mu}$ and the anisotropy axis \mathbf{e}_3 is negligible, and the nanomagnet undergoes a free Larmor precession about the local magnetic field [23, 24]. In the absence of dissipation, this stabilizes the system in full analogy to magnetic trapping of neutral atoms [42, 43]. In Fig. 2 we show the numerical solution of Eqs. (1-5) for nanomagnet dimensions $a = 2b = 20$ nm and the bias field $B_0 = 100$ mT. As evidenced by Fig. 2(a), the magnetization m_x of the particle changes direction. During this change, the mechanical angular momentum l_x changes accordingly in the manifestation of the Einstein–de Haas effect, such that the total angular momentum is conserved. The dynamics observed in Fig. 2(a) is indicative of Gilbert-damping-induced magnetization switching, a process in which the projection of the magnetic moment along the effective magnetic field $\boldsymbol{\omega}_{\text{eff}}/\gamma_0$ changes sign [30]. The timescale of magnetization switching is much shorter than the period of center-of-mass oscillations, here given by $1/\omega_T \sim 10 \mu\text{s}$ [24], thus the nanomagnet shows no signature of confinement [see Fig. 2(b)].

The timescale of levitation in the atom phase is given by the timescale of magnetization switching, and it can be estimated from a simple model as follows. As evidenced by Fig. 2(a-b), the dynamics of the center of mass and the anisotropy axis are approximately constant during switching, such that $\boldsymbol{\omega}_{\text{eff}} \approx \boldsymbol{\omega}_{\text{eff}}(t=0)$. Under this approximation and taking into account that $\eta_G \ll 1$, the magnetic moment projection $m_{\parallel} \equiv \boldsymbol{\omega}_{\text{eff}} \cdot \mathbf{m}/|\boldsymbol{\omega}_{\text{eff}}|$ evolves as

$$\dot{m}_{\parallel} \approx \eta_G [\omega_L + 2\omega_A m_{\parallel}] (1 - m_{\parallel}^2). \quad (6)$$

According to Eq. (6) the component m_{\parallel} exhibits switching if $m_{\parallel}(t=0) \gtrsim -1$ and $\omega_L/2\omega_A > 1$ [30], both of which are fulfilled in the atom phase. Integrating Eq. (6) we obtain the switching time τ [implicitly defined by $m_{\parallel}(\tau) = 0$], which can be well approximated by

$$\tau \approx \frac{\ln(1 + |m_{\parallel}(t=0)|)}{2\eta_G(\omega_L + 2\omega_A)} - \frac{\ln(1 - |m_{\parallel}(t=0)|)}{2\eta_G(\omega_L - 2\omega_A)}. \quad (7)$$

The estimation Eq. (7) is in excellent agreement with

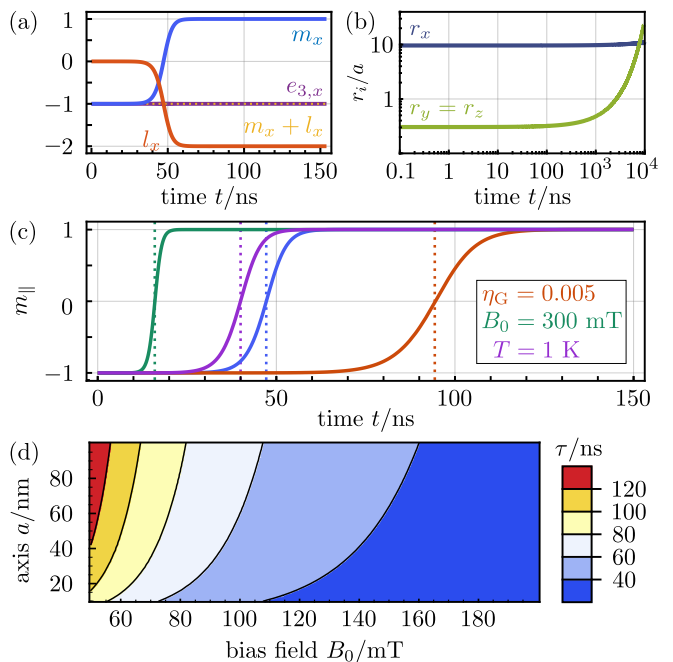


Figure 2. Dynamics in the atom phase for nanomagnet dimensions $a = 2b = 20$ nm and the bias field $B_0 = 100$ mT. Unless otherwise stated, the following values are used: $\eta_G = 10^{-2}$, $T = 10^{-1}$ K, $P = 10^{-2}$ mbar, $\mathcal{M} = 29$ g/mol, and $\alpha_c = 1$. For the remaining parameters the numerical values are given in the caption of Fig. 1(b). (a) Dynamics of the magnetic moment component m_x (blue line), the mechanical angular momentum component l_x (red line), the anisotropy axis component $e_{3,x}$ (purple line) and the total angular momentum (yellow line). (b) Center-of-mass dynamics. (c) Dependence of the magnetization switching on external parameters. Blue line corresponds to the same set of parameters as in (a). Each remaining line differs from the case in (a) by a single parameter, as denoted by the legend. Dotted vertical lines denote the switching time given by Eq. (7). (d) Switching time Eq. (7) as a function of the bias field and the major semi-axis.

the numerical results for several different values of the parameters [see dotted lines in Fig. 2(c)]. In Fig. 2(d) we show the dependence of Eq. (7) on the bias field B_0 and the major semi-axis a . The switching time is always shorter than the center-of-mass oscillation period given by ω_T , and thus no metastability can be observed in the atom phase. In passing, we note that the dissipation due to the background gas has negligible effects, as for the values assumed in Fig. 2(a-c) it occurs on a timescale $\sim 230 - 350 \mu\text{s}$.

Einstein–de Haas phase denotes the regime where $\omega_A, \omega_I \gg \omega_L$, which can be achieved when the dimensions of the nanomagnet are sufficiently small, and the applied bias field is weak. This hierarchy of energy scales manifests in two ways [23, 24]: (i) the anisotropy is strong enough to effectively “lock” the direction of the magnetic moment $\boldsymbol{\mu}$ along the anisotropy axis \mathbf{e}_3 , and (ii) according to the Einstein–de Haas effect, the frequency at which the nanomagnet would rotate if $\boldsymbol{\mu}$ switched direc-

tion is significantly increased at small dimensions, such that switching can be prevented due to energy conservation [4]. In the absence of dissipation, the combination of these two effects stabilizes the system. In Fig. 3 we show the numerical solution of Eqs. (1-5) for nanomagnet dimensions $a = 2b = 2$ nm and the bias field $B_0 = 0.5$ mT. The nanomagnet in the Einstein–de Haas phase is metastable, as evidenced by the confined center-of-mass motion shown in Fig. 3(a). In Fig. 3(b) we show the dynamics of the magnetic moment component m_{\parallel} on the same timescale, which indicates that no magnetization switching occurs in this regime. The absence of switching cannot be simply understood from Eq. (6), because rotation and magnetization dynamics occur on a comparable timescale [see the anisotropy axis oscillations in Fig. 2(c)]. Instead, even in the presence of an anti-aligned magnetic field, Gilbert damping aligns the magnetic moment along the anisotropy axis [see grey arrow in Fig. 3(b)]. This can be explained as follows. We set $\mathbf{m} \equiv \mathbf{e}_3 + \delta\mathbf{m}$ and substitute in Eqs. (1-5). Assuming $|\delta\mathbf{m}| \ll |\mathbf{e}_3|$, we eliminate the magnetic moment degree of freedom to the leading order and obtain the following equation for the correction $\delta\mathbf{m}$,

$$\delta\dot{\mathbf{m}} \approx \omega_{\text{eff}} \times \delta\mathbf{m} - \eta_G [2\omega_A + \omega_0 \mathbf{e}_3 \cdot (\mathbf{m} + \boldsymbol{\ell})] \delta\mathbf{m}, \quad (8)$$

where $\omega_0 \equiv \mu/(\gamma_0 I_0)$, with I_0 the principal moment of inertia along the axis \mathbf{e}_3 . According to Eq. (8), the effect of Gilbert damping is to align \mathbf{m} and \mathbf{e}_3 on a timescale given by $1/(\eta_G \omega_A)$. After this alignment is achieved, the system is stabilized by the magneto-mechanical effects characteristic of the Einstein–de Haas phase.

The main mechanism behind the instability in the Einstein–de Haas phase is thus gas-induced dissipation. In Fig. 3(d-e) we plot the dynamics of the center-of-mass coordinate y and the magnetic moment component m_x on a longer timescale, for two different values of the pressure P . The effect of gas-induced dissipation is to dampen the center-of-mass motion to the equilibrium point, while the magnetic moment moves away from the equilibrium. Both processes happen on a timescale inversely proportional to the pressure P . When $e_x = m_x \approx 0$, the system becomes unstable and ultimately leaves the trap [see grey arrow in Fig. 3(d)]. The metastability of the nanomagnet in the Einstein–de Haas phase is therefore limited by the gas-induced dissipation given by Γ_{rot} , which can be significantly reduced in high vacuum.

We conclude our discussion with several remarks. First, we emphasize that Eqs. (1-5) are deterministic, i.e. they do not account for stochastic terms due to the thermal noise, and are thus appropriate to model the dynamics at sufficiently low temperatures as considered here [8, 44, 45]. In particular, thermal fluctuations of magnetization can be neglected when the magnetic energy exceeds thermal energy, namely when $\mu B_0 \gg k_B T$, with k_B the Boltzmann constant. Similarly, magneto-crystalline thermal fluctuations are suppressed when $k_a V \gg k_B T$. On the other hand, the effect of thermal noise on the center of mass is not negligible in this

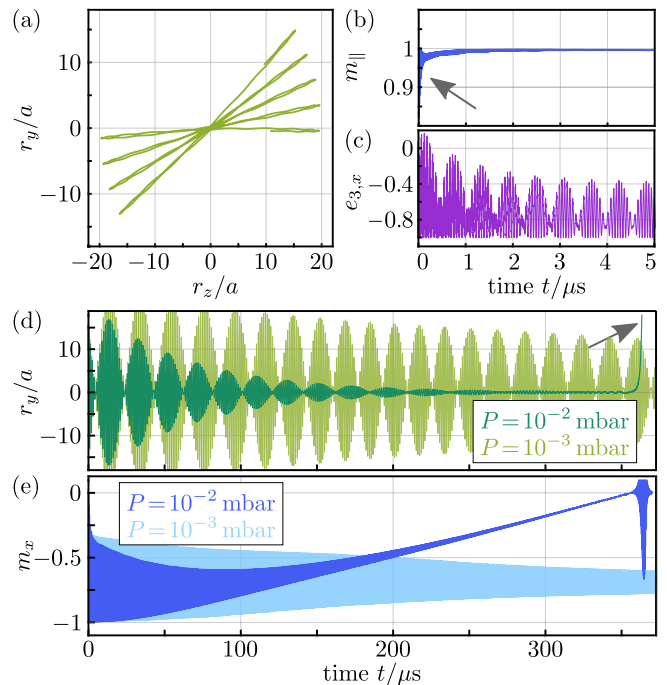


Figure 3. Dynamics in the Einstein–de Haas phase for nanomagnet dimensions $a = 2b = 2$ nm and the bias field $B_0 = 0.5$ mT. Unless otherwise stated, the numerical values of the parameters are the same as in the caption of Fig. 1(b) and Fig. 2. (a) Motion of the system in the y - z plane until time $t_{\text{max}} = 5$ μs . (b) Dynamics of the projection m_{\parallel} . (c) Dynamics of the anisotropy axis component $e_{3,x}$. (d) Center-of-mass dynamics for $P = 10^{-2}$ mbar (dark green) and $P = 10^{-3}$ mbar (light green). (e) Magnetic moment dynamics for $P = 10^{-2}$ mbar (dark blue) and $P = 10^{-3}$ mbar (light blue).

regime [46, 47]. However, at cryogenic conditions and in high vacuum these noises are weak enough not to destroy the deterministic effects captured by Eqs. (1-5) [44]. Second, the initial conditions considered here describe a trapped particle prepared in a thermal equilibrium in the presence of an external loading potential where the center of mass is decoupled from the magnetization and the rotational dynamics. This type of initial conditions can be obtained, for example, by trapping the nanomagnet using Paul traps as in recent experiments [19, 21, 48–56], before releasing it in a Ioffe-Pritchard trap. Third, let us discuss the values of the particle parameters considered in the captions of Fig. 1 and Fig. 2. The material parameters, such as ρ_M , ρ_μ , k_a and η_G , are consistent with Nickel and Cobalt based materials [57–59]. The Gilbert damping parameter η_G could be reduced by considering other materials, for example yttrium iron garnet [60], which could delay magnetization switching and result in metastability in the atom phase. The values of the gas pressure P and the temperature T are experimentally achievable, with numerous recent experiments reaching pressure values as low as $P = 10^{-6}$ mbar [54, 56, 61–64]. Finally, the analysis presented here has been carried out for the case of a non-rotating nanomagnet [65]. The same qualitative behaviour is obtained even in the presence of mechanical

rotation (namely, considering a more general equilibrium configuration with $\ell \neq 0$) (see Appendix D). In particular, the dynamics in the Einstein–de Haas phase remains largely unaffected, provided that the total angular momentum of the system is not zero. In the atom phase, mechanical rotation leads to differences in the switching time τ , as generally expected in the presence of magneto-mechanical coupling [66, 67].

In conclusion, we analyzed how the stability of a nanomagnet levitated in a static magnetic field is affected by the most relevant sources of dissipation. We find that at large applied magnetic fields (atom phase) the system is unstable due to the Gilbert-damping-induced magnetization switching, which occurs on a much faster timescale than the center-of-mass oscillations, thereby preventing the observation of levitation. On the other hand, the system is metastable at weak applied magnetic fields and for small particle dimensions (Einstein–de Haas phase). In this regime, the confinement of the nanomagnet in the magnetic trap is limited only by the gas-induced dissipation, and our results suggest that in high vacuum the timescale of stable levitation can reach and even exceed several hundreds of periods of center-of-mass oscillations. These findings indicate the possibility of observing the phenomenon of quantum spin stabilized magnetic levitation, which we hope will encourage further experimental research. If observed, such phenomenon would not only represent a manifestation of the strong modification that the internal atomic angular momentum has on the mechanical motion of a nanomagnet, but it would also be a step towards controlling and using the rich physics of magnetically levitated nanomagnets.

We thank G. E. W. Bauer, J. J. García-Ripoll, O. Romero-Isart, and B. A. Stickler for helpful discussions. We are grateful to O. Romero-Isart, B. A. Stickler and S. Viola-Kusminskiy for comments on the manuscript. C.C.R. acknowledges funding from ERC Advanced Grant QENOCOBA under the EU Horizon 2020 program (Grant Agreement No. 742102). A.E.R.L. thanks the AMS for the financial support.

-
- [1] A. Einstein and W. J. de Haas, Experimental proof of the existence of Ampère’s molecular currents, *Proc. K. Ned. Akad. Wet.* **18**, 696 (1915).
- [2] O. W. Richardson, A Mechanical Effect Accompanying Magnetization, *Phys. Rev. (Series I)* **26**, 248 (1908).
- [3] S. J. Barnett, Magnetization by Rotation, *Phys. Rev.* **6**, 239 (1915).
- [4] E. M. Chudnovsky, Conservation of angular momentum in the problem of tunneling of the magnetic moment, *Phys. Rev. Lett.* **72**, 3433 (1994).
- [5] C. C. Rusconi and O. Romero-Isart, Magnetic rigid rotor in the quantum regime: Theoretical toolbox, *Phys. Rev. B* **93**, 054427 (2016).
- [6] M. Ganzhorn, S. Klyatskaya, M. Ruben, and W. Wernsdorfer, Quantum Einstein-de Haas effect, *Nature Communications* **7**, 11443 (2016).
- [7] S. Viola Kusminskiy, H. X. Tang, and F. Marquardt, Coupled spin-light dynamics in cavity optomechanics, *Phys. Rev. A* **94**, 033821 (2016).
- [8] H. Keshtgar, S. Streib, A. Kamra, Y. M. Blanter, and G. E. W. Bauer, Magnetomechanical coupling and ferromagnetic resonance in magnetic nanoparticles, *Phys. Rev. B* **95**, 134447 (2017).
- [9] B. A. Stickler, K. Hornberger, and M. S. Kim, Quantum rotations of nanoparticles (2021), [arXiv:2102.00992](https://arxiv.org/abs/2102.00992) [quant-ph].
- [10] M. Perdriat, C. Pellet-Mary, P. Huillery, L. Rondin, and G. Hétet, Spin-mechanics with nitrogen-vacancy centers and trapped particles (2021), [arXiv:2104.10244](https://arxiv.org/abs/2104.10244) [quant-ph].
- [11] D. F. Jackson Kimball, A. O. Sushkov, and D. Budker, Precessing Ferromagnetic Needle Magnetometer, *Phys. Rev. Lett.* **116**, 190801 (2016).
- [12] P. Kumar and M. Bhattacharya, Magnetometry via spin-mechanical coupling in levitated optomechanics, *Opt. Express* **25**, 19568 (2017).
- [13] Y. B. Band, Y. Avishai, and A. Shnirman, Dynamics of a Magnetic Needle Magnetometer: Sensitivity to Landau-Lifshitz-Gilbert Damping, *Phys. Rev. Lett.* **121**, 160801 (2018).
- [14] T. Wang, S. Lourette, S. R. O’Kelley, M. Kayci, Y. Band, D. F. J. Kimball, A. O. Sushkov, and D. Budker, Dynamics of a Ferromagnetic Particle Levitated over a Superconductor, *Phys. Rev. Applied* **11**, 044041 (2019).
- [15] P. Fadeev, C. Timberlake, T. Wang, A. Vinante, Y. B. Band, D. Budker, A. O. Sushkov, H. Ulbricht, and D. F. J. Kimball, Ferromagnetic gyroscopes for tests of fundamental physics, *Quantum Science and Technology* **6**, 024006 (2021).
- [16] P. Fadeev, T. Wang, Y. B. Band, D. Budker, P. W. Graham, A. O. Sushkov, and D. F. J. Kimball, Gravity Probe Spin: Prospects for measuring general-relativistic precession of intrinsic spin using a ferromagnetic gyroscope, *Phys. Rev. D* **103**, 044056 (2021).
- [17] J. Prat-Camps, C. Teo, C. C. Rusconi, W. Wieczorek, and O. Romero-Isart, Ultrasensitive Inertial and Force Sensors with Diamagnetically Levitated Magnets, *Phys. Rev. Applied* **8**, 034002 (2017).
- [18] A. Vinante, P. Falferi, G. Gasbarri, A. Setter, C. Timberlake, and H. Ulbricht, Ultralow Mechanical Damping with Meissner-Levitated Ferromagnetic Microparticles, *Phys. Rev. Applied* **13**, 064027 (2020).
- [19] P. Huillery, T. Delord, L. Nicolas, M. Van Den Bossche, M. Perdriat, and G. Hétet, Spin mechanics with levitating ferromagnetic particles, *Phys. Rev. B* **101**, 134415 (2020).
- [20] J. Gieseler, A. Kabcenell, E. Rosenfeld, J. D. Schaefer, A. Safra, M. J. A. Schuetz, C. Gonzalez-Ballester, C. C. Rusconi, O. Romero-Isart, and M. D. Lukin, Single-Spin Magnetomechanics with Levitated Micromagnets, *Phys. Rev. Lett.* **124**, 163604 (2020).
- [21] T. Delord, P. Huillery, L. Nicolas, and G. Hétet, Spin-cooling of the motion of a trapped diamond, *Nature* **580**, 56 (2020).
- [22] C. Gonzalez-Ballester, J. Gieseler, and O. Romero-Isart, Quantum Acoustomechanics with a Micromagnet, *Phys.*

- Rev. Lett.* **124**, 093602 (2020).
- [23] C. C. Rusconi, V. Pöschhacker, K. Kustura, J. I. Cirac, and O. Romero-Isart, Quantum Spin Stabilized Magnetic Levitation, *Phys. Rev. Lett.* **119**, 167202 (2017).
- [24] C. C. Rusconi, V. Pöschhacker, J. I. Cirac, and O. Romero-Isart, Linear stability analysis of a levitated nanomagnet in a static magnetic field: Quantum spin stabilized magnetic levitation, *Phys. Rev. B* **96**, 134419 (2017).
- [25] M. V. Berry, The LevitronTM: an adiabatic trap for spins, *Proc. R. Soc. Lond. A* **452**, 1207 (1996).
- [26] M. D. Simon, L. O. Heflinger, and S. Ridgway, Spin stabilized magnetic levitation, *American Journal of Physics* **65**, 286 (1997).
- [27] S. Gov, S. Shtrikman, and H. Thomas, On the dynamical stability of the hovering magnetic top, *Physica D: Nonlinear Phenomena* **126**, 214 (1999).
- [28] D. R. Merkin, *Introduction to the Theory of Stability*, Vol. 24 (Springer Science & Business Media, 2012).
- [29] T. L. Gilbert, A phenomenological theory of damping in ferromagnetic materials, *IEEE Transactions on Magnetism* **40**, 3443 (2004).
- [30] G. Bertotti, I. Mayergoyz, and C. Serpico, *Nonlinear magnetization dynamics in nanosystems* (Elsevier, Amsterdam Boston, 2009).
- [31] H. Xi, K.-Z. Gao, Y. Shi, and S. Xue, Precessional dynamics of single-domain magnetic nanoparticles driven by small ac magnetic fields, *Journal of Physics D: Applied Physics* **39**, 4746 (2006).
- [32] L. Martinetz, K. Hornberger, and B. A. Stickler, Gas-induced friction and diffusion of rigid rotors, *Physical Review E* **97**, 052112 (2018).
- [33] T. V. Lyutyy and V. V. Reva, Energy dissipation of rigid dipoles in a viscous fluid under the action of a time-periodic field: The influence of thermal bath and dipole interaction, *Phys. Rev. E* **97**, 052611 (2018).
- [34] S. Chikazumi and C. D. Graham, *Physics of Ferromagnetism 2e*, Vol. 94 (Oxford University Press on Demand, 2009).
- [35] D. Gatteschi, R. Sessoli, and J. Villain, *Molecular nanomagnets* (Oxford University Press, 2006).
- [36] The total internal angular momentum \mathbf{F} is a sum of the individual atomic angular momenta (spin and orbital), which contribute to the atomic magnetic moment. For a single domain magnetic particle, it is customary to assume that \mathbf{F} can be described as a vector of constant magnitude, $|\mathbf{F}| = \mu/\gamma_0$ (macrospin approximation) [35].
- [37] We remark that different magnetic traps, provided they have a non-zero bias field, should result in similar qualitative behaviour.
- [38] J. Reichel and V. Vuletic, *Atom chips* (John Wiley & Sons, 2011).
- [39] The expressions for $\Gamma_{\text{cm,rot}}$ for a cylindrical particle capture the order of magnitude of the dissipation rates for a spheroidal particle [68, 69].
- [40] J. Taylor, *Classical mechanics* (University Science Books, Mill Valley, California, 2005).
- [41] J. Miltat, G. Albuquerque, and A. Thiaville, An Introduction to Micromagnetics in the Dynamic Regime, in *Spin Dynamics in Confined Magnetic Structures I*, edited by B. Hillebrands and K. Ounadjela (Springer Berlin Heidelberg, Berlin, Heidelberg, 2002) pp. 1–33.
- [42] C. Sukumar and D. Brink, Spin-flip transitions in a magnetic trap, *Physical review A* **56**, 2451 (1997).
- [43] D. Brink and C. Sukumar, Majorana spin-flip transitions in a magnetic trap, *Physical Review A* **74**, 035401 (2006).
- [44] T. V. Lyutyy, S. I. Denisov, and P. Hänggi, Dissipation-induced rotation of suspended ferromagnetic nanoparticles, *Phys. Rev. B* **100**, 134403 (2019).
- [45] W. F. Brown, Thermal Fluctuations of a Single-Domain Particle, *Phys. Rev.* **130**, 1677 (1963).
- [46] O. Romero-Isart, Coherent inflation for large quantum superpositions of levitated microspheres, *New Journal of Physics* **19**, 123029 (2017).
- [47] H. Pino, J. Prat-Camps, K. Sinha, B. P. Venkatesh, and O. Romero-Isart, On-chip quantum interference of a superconducting microsphere, *Quantum Science and Technology* **3**, 025001 (2018).
- [48] J. Millen, P. Z. G. Fonseca, T. Mavrogordatos, T. S. Monteiro, and P. F. Barker, Cavity Cooling a Single Charged Levitated Nanosphere, *Phys. Rev. Lett.* **114**, 123602 (2015).
- [49] I. Alda, J. Berthelot, R. A. Rica, and R. Quidant, Trapping and manipulation of individual nanoparticles in a planar Paul trap, *Applied Physics Letters* **109**, 163105 (2016).
- [50] G. P. Conangla, A. W. Schell, R. A. Rica, and R. Quidant, Motion Control and Optical Interrogation of a Levitating Single Nitrogen Vacancy in Vacuum, *Nano Letters* **18**, 3956 (2018).
- [51] T. Delord, P. Huillery, L. Schwab, L. Nicolas, L. Lecordier, and G. Hétet, Ramsey Interferences and Spin Echoes from Electron Spins Inside a Levitating Macroscopic Particle, *Phys. Rev. Lett.* **121**, 053602 (2018).
- [52] T. M. Ostermayr, J. Gebhard, D. Haffa, D. Kiefer, C. Kreuzer, K. Allinger, C. Bömer, J. Braenzel, M. Schnürer, I. Cermak, J. Schreiber, and P. Hilz, A transportable Paul-trap for levitation and accurate positioning of micron-scale particles in vacuum for laser-plasma experiments, *Review of Scientific Instruments* **89**, 013302 (2018).
- [53] H. L. Partner, J. Zoll, A. Kuhlicke, and O. Benson, Printed-circuit-board linear Paul trap for manipulating single nano- and microparticles, *Review of Scientific Instruments* **89**, 083101 (2018).
- [54] D. S. Bykov, P. Mestres, L. Dania, L. Schmöger, and T. E. Northup, Direct loading of nanoparticles under high vacuum into a Paul trap for levitodynamical experiments, *Applied Physics Letters* **115**, 034101 (2019).
- [55] G. P. Conangla, R. A. Rica, and R. Quidant, Extending Vacuum Trapping to Absorbing Objects with Hybrid Paul-Optical Traps, *Nano Letters* **20**, 6018 (2020).
- [56] L. Dania, D. S. Bykov, M. Knoll, P. Mestres, and T. E. Northup, Optical and electrical feedback cooling of a silica nanoparticle levitated in a Paul trap, *Phys. Rev. Research* **3**, 013018 (2021).
- [57] J. Walowski, M. D. Kaufmann, B. Lenk, C. Hamann, J. McCord, and M. Münzenberg, Intrinsic and non-local Gilbert damping in polycrystalline nickel studied by Ti: sapphire laser fs spectroscopy, *Journal of Physics D: Applied Physics* **41**, 164016 (2008).
- [58] E. Barati, M. Cinal, D. M. Edwards, and A. Umerski, Gilbert damping in magnetic layered systems, *Phys. Rev. B* **90**, 014420 (2014).
- [59] C. Papusoi, T. Le, C. C. H. Lo, C. Kaiser, M. Desai, and R. Acharya, Measurements of Gilbert damping parameter α for CoPt-based and CoFe-based films for mag-

netic recording applications, *Journal of Physics D: Applied Physics* **51**, 325002 (2018).

- [60] S. Klingler, H. Maier-Flaig, C. Dubs, O. Surzhenko, R. Gross, H. Huebl, S. T. B. Goennenwein, and M. Weiler, Gilbert damping of magnetostatic modes in a yttrium iron garnet sphere, *Applied Physics Letters* **110**, 092409 (2017).
- [61] N. Meyer, A. d. I. R. Sommer, P. Mestres, J. Gieseler, V. Jain, L. Novotny, and R. Quidant, Resolved-Sideband Cooling of a Levitated Nanoparticle in the Presence of Laser Phase Noise, *Phys. Rev. Lett.* **123**, 153601 (2019).
- [62] D. Windey, C. Gonzalez-Ballester, P. Maurer, L. Novotny, O. Romero-Isart, and R. Reimann, Cavity-Based 3D Cooling of a Levitated Nanoparticle via Coherent Scattering, *Phys. Rev. Lett.* **122**, 123601 (2019).
- [63] U. Delić, M. Reisenbauer, K. Dare, D. Grass, V. Vuletić, N. Kiesel, and M. Aspelmeyer, Cooling of a levitated nanoparticle to the motional quantum ground state, *Science* **367**, 892 (2020).
- [64] A. de los Ríos Sommer, N. Meyer, and R. Quidant, Strong optomechanical coupling at room temperature by coherent scattering, *Nature Communications* **12**, 276 (2021).
- [65] Rotational cooling might be needed to unambiguously identify the internal spin as the source of stabilization. Sub-Kelvin cooling of nanorotor has been recently achieved [70, 71], and cooling to micro-K should be possible [69].
- [66] A. A. Kovalev, G. E. W. Bauer, and A. Brataas, Nanomechanical Magnetization Reversal, *Phys. Rev. Lett.* **94**, 167201 (2005).
- [67] T. Taniguchi, Magnetization reversal condition for a nanomagnet within a rotating magnetic field, *Phys. Rev. B* **90**, 024424 (2014).
- [68] L. Martinetz, K. Hornberger, J. Millen, M. S. Kim, and B. A. Stickler, Quantum electromechanics with levitated nanoparticles, *npj Quantum Inf.* **6**, 101 (2020).
- [69] J. Schäfer, H. Rudolph, K. Hornberger, and B. A. Stickler, Cooling nanorotors by elliptic coherent scattering, *Phys. Rev. Lett.* **126**, 163603 (2021).
- [70] F. van der Laan, R. Reimann, A. Militaru, F. Tebbenjohanns, D. Windey, M. Frimmer, and L. Novotny, Optically levitated rotor at its thermal limit of frequency stability, *Phys. Rev. A* **102**, 013505 (2020).
- [71] F. van der Laan, R. Reimann, F. Tebbenjohanns, J. Vijayan, L. Novotny, and M. Frimmer, Observation of radiation torque shot noise on an optically levitated nanodumbbell (2021), [arXiv:2012.14231](https://arxiv.org/abs/2012.14231) [physics.optics].

Appendix A: Rotation to the body frame

In this section we define the transformation matrix between the body-fixed and the laboratory reference frames according to the ZYZ Euler angle convention, with the Euler angles denoted as $\mathbf{\Omega} = (\alpha, \beta, \gamma)^T$. We define the transformation between the laboratory frame $O\mathbf{e}_x\mathbf{e}_y\mathbf{e}_z$ and the body frame $O\mathbf{e}_1\mathbf{e}_2\mathbf{e}_3$ as follows,

$$\begin{pmatrix} \mathbf{e}_1 \\ \mathbf{e}_2 \\ \mathbf{e}_3 \end{pmatrix} = R(\mathbf{\Omega}) \begin{pmatrix} \mathbf{e}_x \\ \mathbf{e}_y \\ \mathbf{e}_z \end{pmatrix}, \quad (\text{A1})$$

where

$$R(\mathbf{\Omega}) \equiv R_z(\alpha)R_y(\beta)R_z(\gamma) = \begin{pmatrix} \cos \gamma & \sin \gamma & 0 \\ -\sin \gamma & \cos \gamma & 0 \\ 0 & 0 & 1 \end{pmatrix} \begin{pmatrix} \cos \beta & 0 & -\sin \beta \\ 0 & 1 & 0 \\ -\sin \beta & 0 & \cos \beta \end{pmatrix} \begin{pmatrix} \cos \alpha & \sin \alpha & 0 \\ -\sin \alpha & \cos \alpha & 0 \\ 0 & 0 & 1 \end{pmatrix}. \quad (\text{A2})$$

Accordingly, the components v_j ($j = 1, 2, 3$) of a vector \mathbf{v} in the body frame $O\mathbf{e}_1\mathbf{e}_2\mathbf{e}_3$ and the components v_ν ($\nu = x, y, z$) of the same vector in the laboratory frame $O\mathbf{e}_x\mathbf{e}_y\mathbf{e}_z$ are related as

$$\begin{pmatrix} v_1 \\ v_2 \\ v_3 \end{pmatrix} = R^T(\mathbf{\Omega}) \begin{pmatrix} v_x \\ v_y \\ v_z \end{pmatrix}. \quad (\text{A3})$$

The angular velocity of a rotating particle $\boldsymbol{\omega}$ can be written in terms of the Euler angles as $\boldsymbol{\omega} = \dot{\alpha}\mathbf{e}_z + \dot{\beta}\mathbf{e}'_y + \dot{\gamma}\mathbf{e}_3$, where $(\mathbf{e}'_x, \mathbf{e}'_y, \mathbf{e}'_z)^T = R(\alpha)(\mathbf{e}_x, \mathbf{e}_y, \mathbf{e}_z)^T$ denotes the frame $O\mathbf{e}'_x\mathbf{e}'_y\mathbf{e}'_z$ obtained after the first rotation of the laboratory frame $O\mathbf{e}_x\mathbf{e}_y\mathbf{e}_z$ in the ZYZ convention. By using (A1) and (A2), we can rewrite angular velocity in terms of the body frame coordinates,

$$\boldsymbol{\omega} = \dot{\alpha} \left[R(\mathbf{\Omega})^{-1} \begin{pmatrix} \mathbf{e}_1 \\ \mathbf{e}_2 \\ \mathbf{e}_3 \end{pmatrix} \right]_3 + \dot{\beta} \left[R(\gamma)^{-1} \begin{pmatrix} \mathbf{e}_1 \\ \mathbf{e}_2 \\ \mathbf{e}_3 \end{pmatrix} \right]_2 + \dot{\gamma}\mathbf{e}_3, \quad (\text{A4})$$

which is compactly written as $(\omega_1, \omega_2, \omega_3)^T = A(\mathbf{\Omega})\dot{\mathbf{\Omega}}$, with

$$A(\mathbf{\Omega}) = \begin{pmatrix} -\cos \gamma \sin \beta & \sin \gamma & 0 \\ \sin \beta \sin \gamma & \cos \gamma & 0 \\ \cos \beta & 0 & 1 \end{pmatrix}. \quad (\text{A5})$$

Appendix B: Hamiltonian of a levitated nanomagnet

In this section we summarize the description of the dynamics of a levitated nanomagnet in the Lagrangian formalism, and we derive the classical Hamiltonian function.

The mechanical motion of the nanomagnet is described by the center-of-mass position \mathbf{r} and the velocity $\dot{\mathbf{r}}$, as well as its angular orientation $\mathbf{\Omega}$ and angular velocity $\dot{\mathbf{\Omega}} = (\dot{\alpha}, \dot{\beta}, \dot{\gamma})^T$. The orientation of the nanomagnet is described by the body-fixed reference frame $O\mathbf{e}_1\mathbf{e}_2\mathbf{e}_3$ which is obtained from the laboratory frame $O\mathbf{e}_x\mathbf{e}_y\mathbf{e}_z$ according to Eq. (A1). The body-fixed frame is chosen such that \mathbf{e}_3 coincides with the magnetocrystalline anisotropy axis, which we assume to be along the major semi-axis a [34]. We assume that the magnetic response of the nanomagnet is approximated by a point dipole with the magnetic moment $\boldsymbol{\mu}$ of a constant magnitude, such that its components in the laboratory frame

are $\boldsymbol{\mu} = \mu(\cos\phi \sin\theta, \sin\phi \sin\theta, \cos\theta)^T$, with ϕ, θ the polar and azimuthal angles.

The conservative dynamics of a nanomagnet levitated in a static magnetic field $\mathbf{B}(\mathbf{r})$ is modelled by a Lagrangian [24]

$$\begin{aligned} \mathcal{L} = & \frac{1}{2}M\dot{\mathbf{r}}^2 + \frac{I_0}{2}(\dot{\gamma}^2 + \dot{\alpha}^2 \cos^2\beta + 2\dot{\alpha}\dot{\gamma} \cos\beta) \\ & + \frac{I_1}{2}(\dot{\beta}^2 + \dot{\alpha}^2 \sin^2\beta) + \boldsymbol{\mu} \cdot \mathbf{B}(\mathbf{r}) + k_a V \left[\frac{\boldsymbol{\mu}}{\mu} \cdot \mathbf{e}_3(\boldsymbol{\Omega}) \right]^2 \\ & - \frac{\mu}{\gamma_0} \dot{\phi} \cos\theta. \end{aligned} \quad (\text{B1})$$

Here M is the mass of the nanomagnet, $I_0 \equiv 2Mb^2/5$ and $I_1 \equiv M(a^2 + b^2)/5$ are principal moments of inertia, k_a is the anisotropy energy density of the material [35], V is the volume of the nanomagnet, and γ_0 is the gyromagnetic ratio of the material. The first term in Eq. (B1) describes the kinetic energy of the center of mass, while the second and the third term describe the rotational kinetic energy. The last two terms in the second line of Eq. (B1) denote, respectively, the magnetic dipole interaction and the uniaxial anisotropy interaction. The last term in Eq. (B1) accounts for the kinetic energy associated to the motion of the magnetic moment [41], and it leads to the phenomenological Landau-Lifshitz-Gilbert equations describing the magnetization dynamics [31, 41].

The Hamiltonian can be obtained from Eq. (B1) by a Legendre transformation, $\mathcal{H} = \sum_i P_i Q_i - \mathcal{L}$, where $\mathbf{Q} \equiv \{\mathbf{r}, \boldsymbol{\Omega}, \phi\}$, and $\mathbf{P} \equiv \{\mathbf{p}, \mathbf{p}_\Omega, p_\phi\}$ are the conjugate momenta given by $P_i = \partial\mathcal{L}/\partial\dot{Q}_i$, namely $\mathbf{p} = M\dot{\mathbf{r}}$, $p_\phi = -\mu \cos\theta/\gamma_0$, and $\mathbf{p}_\Omega = G(\boldsymbol{\Omega})\dot{\boldsymbol{\Omega}}$, with

$$G(\boldsymbol{\Omega}) = \begin{pmatrix} I_0 \cos^2\beta + I_1 \sin^2\beta & 0 & I_0 \cos\beta \\ 0 & I_1 & 0 \\ I_0 \cos\beta & 0 & I_0 \end{pmatrix}. \quad (\text{B2})$$

It is convenient to express the Hamiltonian in terms of the mechanical angular momentum components in the body frame, $\mathbf{L} = (L_1, L_2, L_3)^T$, as follows. The angular velocity of the nanomagnet is given by $\boldsymbol{\omega} \equiv I^{-1}\mathbf{L}$, with I the tensor of inertia, which in the body frame reads $I = \text{diag}(I_1, I_1, I_0)$. On the other hand, the body-frame components of the angular velocity $\boldsymbol{\omega}$ are related to the Euler angles using Eq. (A5). Consequently, the rotational conjugate momenta \mathbf{p}_Ω can be written in terms of the body-frame components of \mathbf{L} as $\mathbf{p}_\Omega = [IA(\boldsymbol{\Omega})G^{-1}(\boldsymbol{\Omega})]^{-1}\mathbf{L}$. The Hamiltonian of a levitated nanomagnet can thus be written as

$$\mathcal{H} = \frac{\mathbf{p}^2}{2M} + \frac{1}{2}\mathbf{L}I^{-1}\mathbf{L} - \boldsymbol{\mu} \cdot \mathbf{B}(\mathbf{r}) - k_a V \left[\frac{\boldsymbol{\mu}}{\mu} \cdot \mathbf{e}_3(\boldsymbol{\Omega}) \right]^2. \quad (\text{B3})$$

From Eq. (B3) we can obtain equations of motion for any function $f(Q_i, P_i)$ using Poisson brackets, as $\dot{f} = \{f, H\}$,

where

$$\begin{aligned} \{f, g\} = & \sum_{i=1}^6 \left(\frac{\partial f}{\partial Q_i} \frac{\partial g}{\partial P_i} - \frac{\partial g}{\partial P_i} \frac{\partial f}{\partial Q_i} \right) + \\ & \frac{\gamma_0/\mu}{\sin\theta} \left(\frac{\partial f}{\partial\phi} \frac{\partial g}{\partial\theta} - \frac{\partial g}{\partial\theta} \frac{\partial f}{\partial\phi} \right). \end{aligned} \quad (\text{B4})$$

Using Poisson brackets we derive equations of motion given by the Hamiltonian Eq. (B3),

$$\begin{aligned} \dot{\mathbf{r}} &= \mathbf{p}/M, & \dot{\mathbf{p}} &= \nabla_{\mathbf{r}}[\boldsymbol{\mu} \cdot \mathbf{B}(\mathbf{r})], \\ \dot{\mathbf{e}}_3 &= \boldsymbol{\omega} \times \mathbf{e}_3, & \dot{\mathbf{L}} &= [\gamma_0 \mathbf{B}(\mathbf{r}) + \boldsymbol{\omega}_{\text{eff}}] \times \boldsymbol{\mu}, \\ \dot{\boldsymbol{\mu}} &= -\boldsymbol{\omega}_{\text{eff}} \times \boldsymbol{\mu}, \end{aligned} \quad (\text{B5})$$

with $\boldsymbol{\omega}_{\text{eff}} \equiv 2(k_a V \gamma_0 / \mu^2)(\boldsymbol{\mu} \cdot \mathbf{e}_3)\mathbf{e}_3 + \gamma_0 \mathbf{B}(\mathbf{r})$.

Appendix C: Thermal initial conditions

In this section we obtain the initial conditions for the dynamics of the nanomagnet. We assume that the nanomagnet is prepared in the thermal state of \mathcal{H}_{aux} at the temperature T , with an auxiliary loading potential given by the Hamiltonian $\mathcal{H}_{\text{aux}} = \mathcal{H}_{\text{cm}} + \mathcal{H}_{\text{rot}} + \mathcal{H}_\mu$. Here $\mathcal{H}_{\text{cm}} \equiv \mathbf{p}^2/(2M) + M[\omega_X^2 r_x^2 + \omega_T^2(r_y^2 + r_z^2)]/2$, where we take $\omega_X^2 = \mu B''/M$ and $\omega_T^2 = \mu(B''^2 - B_0 B''/2)/(MB_0)$ in agreement with the typical trapping frequencies in a Ioffe-Pritchard field [38], $\mathcal{H}_{\text{rot}} \equiv \mathbf{L}I^{-1}\mathbf{L}/2 - k_a V e_{3,x}^2$ and $\mathcal{H}_\mu \equiv -\mu_x B_0 = -\mu B_0 \cos\theta$. For the degrees of freedom $\mathbf{x} \equiv (\mathbf{r}, \mathbf{p}, \mathbf{p}_\Omega, \mu_x)^T$ we take as the initial displacement from the equilibrium the corresponding standard deviation, given by $\Delta x_i = (\langle x_i^2 \rangle - \langle x_i \rangle^2)^{1/2}$, where $\langle x_i^k \rangle = Z^{-1} \int d\mathbf{x} x_i^k \exp[-\mathcal{H}_{\text{aux}}/(k_B T)]$, with $k = 1, 2$ and the partition function Z , which can be written as $Z \equiv Z_{\text{cm}} Z_{\text{rot}} Z_\mu$. For the Euler angles $\boldsymbol{\Omega}$ we use a modified definition for the initial displacements, as shown below. The corresponding values for the anisotropy axis \mathbf{e}_3 and the mechanical angular momentum \mathbf{L} are obtained from $\boldsymbol{\Omega}$ and \mathbf{p}_Ω using Eq. (A1) and Eq. (B2), respectively.

The partition function Z_μ is given by the Hamiltonian \mathcal{H}_μ and it reads $Z_\mu = 4\pi(\sinh\xi)/\xi$, where $\xi \equiv \mu B_0/(k_B T)$ and k_B is the Boltzmann constant. Defining a dimensionless variable $\mathbf{m} \equiv \boldsymbol{\mu}/\mu$, the mean values are given by $\langle m_x \rangle = \partial \ln Z_\mu / \partial \xi$ and $\langle m_x^2 \rangle = (\partial^2 Z_\mu / \partial \xi^2) / Z_\mu$, such that the variance reads $\Delta^2 m_x = 1/\xi^2 - (\sinh^{-1}\xi)^2$. For the remaining components of the magnetic moment we set as the initial displacements $\Delta^2 m_y = (1 - \Delta^2 m_x)^{1/2}$ and $\Delta m_z = 0$, such that the norm is preserved, namely $|\mathbf{m}(t=0)| = 1$. In Fig. 4(a) we plot the value of Δm_x as a function of the temperature T , for two different regimes of parameters: Einstein-de Haas phase with $a = 2b = 2$ nm and $B_0 = 0.5$ mT (red line) and atom phase with $a = 2b = 20$ nm and $B_0 = 100$ mT (blue line).

The partition function Z_{cm} is given by the Hamiltonian \mathcal{H}_{cm} and it reads $Z_{\text{cm}} = (2\pi k_B T)^3 / (\omega_X \omega_T^2)$. The variances follow as $\Delta^2 r_i = k_B T / M \omega_i^2$ and $\Delta^2 p_i = M k_B T$, with $i = x, y, z$ and $\omega_y = \omega_z = \omega_T$. In Fig. 4(b) we

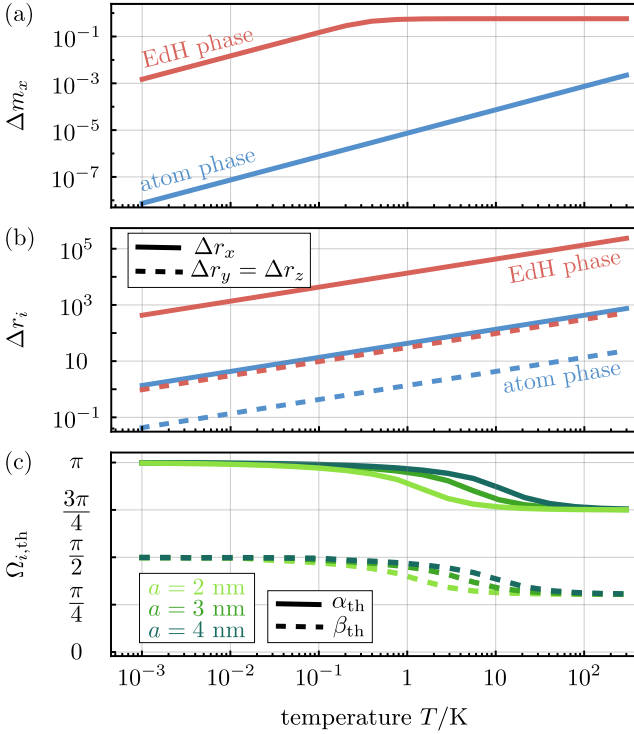


Figure 4. (a) Temperature dependence of the magnetic moment standard deviation in the thermal state, for the nanomagnet in the Einstein–de Haas phase with $a = 2b = 2$ nm, $B_0 = 0.5$ mT (red line), and in the atom phase with $a = 2b = 20$ nm and $B_0 = 100$ mT (blue line). For the remaining parameters the numerical values are given in the caption of Fig. 1(b). (b) Temperature dependence of the center-of-mass standard deviations in the thermal state, for the same parameters as in (a). (c) Temperature dependence of the Euler angles α_{th} and β_{th} for different values of the major semi-axis a , and $b = a/2$. For the remaining parameters the numerical values are as in (a-b).

plot the values of Δr_i as a function of the temperature T , for the same regimes of parameters as in panel (a). At cryogenic temperatures the displacements of the center of mass given by the thermal state are small enough such that the Ioffe-Pritchard approximation of the static magnetic field is valid [5, 38].

The partition function Z_{rot} is given by the Hamiltonian \mathcal{H}_{rot} , which can be written in terms of the canonical coordinates $\mathbf{\Omega}$, \mathbf{p}_{Ω} as

$$\mathcal{H}_{\text{rot}} = \frac{p_{\beta}^2}{2I_1} + \frac{p_{\gamma}^2}{2I_0} + \frac{(p_{\alpha} - p_{\gamma} \cos \beta)^2}{2I_1 \sin^2 \beta} - k_a V (\cos \alpha \sin \beta)^2. \quad (\text{C1})$$

The partition function reads $Z_{\text{rot}} = 2\pi(2\pi k_B T)^{3/2} (I_1^2 I_0)^{1/2} \mathcal{I}[1]$, where we define a functional

$$f(\alpha, \beta) \mapsto \mathcal{I}[f(\alpha, \beta)] = \int_0^{2\pi} d\alpha \int_0^{\pi} d\beta f(\alpha, \beta) \sin \beta e^{\frac{k_a V}{k_B T} (\cos \alpha \sin \beta)^2}, \quad (\text{C2})$$

with $f(\alpha, \beta)$ an arbitrary function. Note that the mean value of $f(\alpha, \beta)$ can be written as $\langle f(\alpha, \beta) \rangle = \mathcal{I}[f(\alpha, \beta)] / \mathcal{I}[1]$. The variances follow as

$$\Delta^2 p_{\alpha} = I_1 k_B T \left[1 - \frac{I_1 - I_0}{I_1} \langle \cos^2 \beta \rangle \right], \quad (\text{C3})$$

$$\Delta^2 p_{\beta} = I_1 k_B T, \quad \Delta^2 p_{\gamma} = I_0 k_B T.$$

Finally, for the angles $\mathbf{\Omega}$ we use a modified definition of their mean values in the thermal state, which we denote as $\mathbf{\Omega}_{\text{th}}$ and obtain as $\alpha_{\text{th}} \equiv \cos^{-1}[-\sqrt{\langle \cos^2 \alpha \rangle}]$, $\beta_{\text{th}} \equiv \cos^{-1}[\sqrt{\langle \cos^2 \beta \rangle}]$ and $\gamma_{\text{th}} = \cos^{-1}[\sqrt{\langle \cos^2 \gamma \rangle}] = \pi/4$. In Fig. 4(c) we plot the angles α_{th} and β_{th} as a function of the temperature T for different values of the major semi-axis a , and $b = a/2$. The factor $k_a V / (k_B T)$ in the exponential in Eq. (C2) implies that larger particles require higher temperatures to be significantly displaced out of the equilibrium configuration. For cryogenic temperatures and particle dimensions considered in the main text, it is therefore appropriate to approximate $\alpha_{\text{th}} \approx \pi$, $\beta_{\text{th}} \approx \pi/2$ and $\Delta^2 p_{\alpha} \approx I_1 k_B T$.

Appendix D: Dynamics in the presence of rotation

In this section we consider a more general equilibrium configuration, namely a nanomagnet initially rotating such that in the equilibrium point $\mathbf{L} = -I_0 \omega_S \mathbf{e}_x$, with the sign convention such that $\omega_S > 0$ denotes the rotation in the clockwise direction. This equilibrium point is linearly stable in the absence of dissipation [23, 24], and an example of a stability diagram with $|\omega_S|/2\pi = 100$ MHz is shown in Fig. 5(a), both in the clockwise (left panel) and counterclockwise (right panel) direction. Apart from the Einstein–de Haas and the atom phase, the stability diagram displays an additional stable region in which the system is stabilized by the mechanical rotation, analogously to the classical magnetic top [25–27]. The two cases considered in the main text are denoted in Fig. 5(a) by yellow and green points (Einstein–de Haas and atom phase, respectively). Here we consider how the dynamics in these two cases is modified by the rotation ω_S . In Fig. 5(b) we show the motion in the y - z plane in the Einstein–de Haas phase for both directions of rotation. This can be compared with Fig. 3(a). The rotation does not qualitatively affect the dynamics of the system. The difference in the two trajectories can be explained by a different total angular momentum in the two cases, as in the case of a clockwise (counterclockwise) rotation the mechanical and the internal angular momentum are parallel (anti-parallel), such that the total angular momentum is increased (decreased) compared to the non-rotating case. This asymmetry arises from the stability diagram of a rotating nanomagnet [compare with Fig. 5(a)], and it is not a consequence of dissipation. In Fig. 5(c) we show the dynamics of the component m_{\parallel} in the atom phase. The rotation has a slight effect on the switching time τ , shifting it forwards (backwards) in case

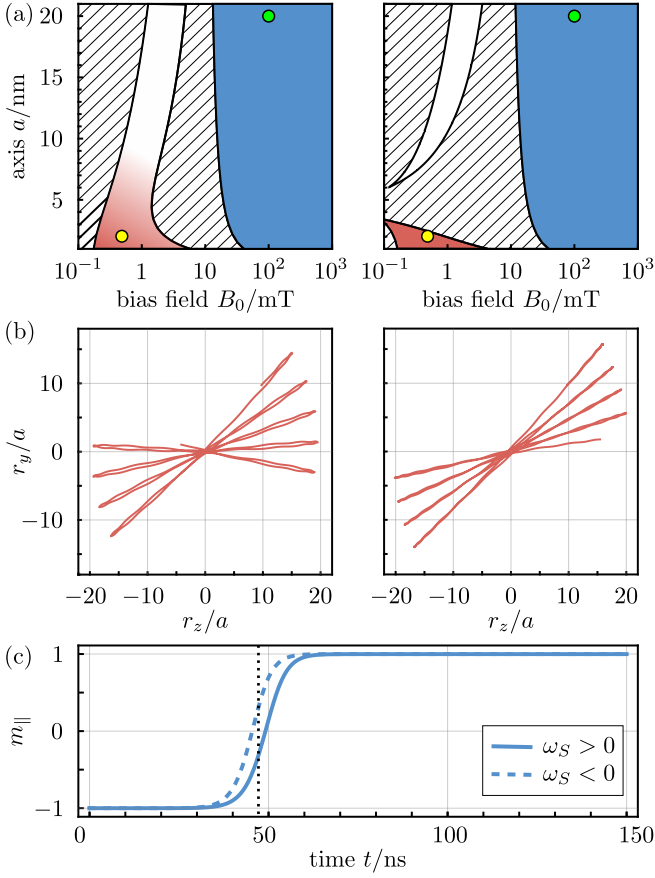


Figure 5. Dynamics of a nanomagnet initially rotating around the axis \mathbf{e}_x with the frequency ω_S . (a) Stability diagram in the absence of dissipation for $|\omega_S|/2\pi = 100$ MHz. Left panel: Clockwise rotation ($\omega_S > 0$). Right panel: counterclockwise rotation ($\omega_S < 0$). For the remaining parameters the numerical values are given in the caption of Fig. 1(b). (b) Motion in the y - z plane for the rotating nanomagnet in the Einstein–de Haas phase [denoted by yellow points in (a)], using the same numerical values of the parameters as in Fig. 3(a). Left panel: Clockwise rotation. Right panel: counterclockwise rotation. (c) Magnetization switching for the rotating nanomagnet in the atom phase [denoted by green points in (a)], using the same numerical values of the parameters as in Fig. 2(a). Solid line: clockwise rotation. Dashed line: counterclockwise rotation. Dotted vertical line denotes the switching time given by Eq. (7).

of a clockwise (counterclockwise) rotation. This is generally expected in the presence of magneto-mechanical coupling [66, 67].